REPORT DOCUMENTATION PAGE

Form Approved OMB NO. 0704-0188

1. REPORT DATE (DD-MM-YYYY)	2. REPORT TYPE	3. DATES COVERED (From - To)
23-01-2016	Final Report	1-Jul-2012 - 30-Jun-2015

4. TITLE AND SUBTITLE

Final Report: Ultra-high Thermal Conductivity of Spider Silk: Protein Function Study with Controlled Structure Change and Comparison

5a. CONTRACT NUMBER
W911NF-12-1-0272

5b. GRANT NUMBER

5c. PROGRAM ELEMENT NUMBER
611102

6. AUTHORS
Xinwei Wang, Cheryl Hayashi

5d. PROJECT NUMBER

5e. TASK NUMBER

5f. WORK UNIT NUMBER

7. PERFORMING ORGANIZATION NAMES AND ADDRESSES
Iowa State University of Science and Techn
1138 Pearson Hall

Ames, IA 50011 -2207

8. PERFORMING ORGANIZATION REPORT NUMBER

9. SPONSORING/MONITORING AGENCY NAME(S) AND ADDRESS (ES)
U.S. Army Research Office
P.O. Box 12211
Research Triangle Park, NC 27709-2211

10. SPONSOR/MONITOR'S ACRONYM(S)
ARO

11. SPONSOR/MONITOR'S REPORT NUMBER(S)
61825-LS.21

12. DISTRIBUTION AVAILIBILITY STATEMENT
Approved for Public Release; Distribution Unlimited

13. SUPPLEMENTARY NOTES
The views, opinions and/or findings contained in this report are those of the author(s) and should not contrued as an official Department of the Army position, policy or decision, unless so designated by other documentation.

14. ABSTRACT
In the past three years, we have conducted extensive research to study the structure of spider silks and investigate how the structure affects the silk's thermal transport. The comparison of thermal conductivity (k) and structural information between the naturally spun and manually spun spider silks demonstrates that the alignment of the antiparallel beta-sheet crystals in spider silks plays one of the most important roles in improving thermal transport. Various structural manipulations have been introduced by casting the silk protein into different shapes, varying the speed of manual silk spinning, using different silks from the same spider and silks from different types of spiders

15. SUBJECT TERMS
Crystallite size, XRD, thermal reffusivity, phonon scattering, thermal conductivity, structural effect, 3D anisotropic

16. SECURITY CLASSIFICATION OF:			17. LIMITATION OF ABSTRACT	15. NUMBER OF PAGES	19a. NAME OF RESPONSIBLE PERSON
a. REPORT	b. ABSTRACT	c. THIS PAGE			Xinwei Wang
UU	UU	UU	UU		19b. TELEPHONE NUMBER 515-294-2085

Report Title

Final Report: Ultra-high Thermal Conductivity of Spider Silk: Protein Function Study with Controlled Structure Change and Comparison

ABSTRACT

In the past three years, we have conducted extensive research to study the structure of spider silks and investigate how the structure affects the silk's thermal transport. The comparison of thermal conductivity (k) and structural information between the naturally spun and manually spun spider silks demonstrates that the alignment of the antiparallel beta-sheet crystals in spider silks plays one of the most important roles in improving thermal transport. Various structural manipulations have been introduced by casting the silk protein into different shapes, varying the speed of manual silk spinning, using different silks from the same spider and silks from different types of spiders. The thin width of silks has been proved to significantly improve k. The silks from the spiders in unhealthy conditions also showed a higher k. Rough structures would enhance phonon scattering and thus lower k. A small range of the variation of the spinning rate in producing spider silks would not obviously increase k, when no significant shape change is induced. The organic solvent in silver paste involved in our experiment has little effect in decreasing k. On the other hand, to go deeper into the nanoscale nature of the structure of spider silks, X-ray diffraction (XRD) has been employed to study the crystallite size of spider silks. Also a lab-developed thermal reffusivity theory has been employed to study thermal properties of spider silks at low temperatures down to 10 K. The crystallite size obtained through XRD and mean free path of the defect-induced phonon scattering are nicely consistent with each other.

Enter List of papers submitted or published that acknowledge ARO support from the start of the project to the date of this printing. List the papers, including journal references, in the following categories:

(a) Papers published in peer-reviewed journals (N/A for none)

Received		Paper
08/28/2013	1.00	Huan Lin, Shen Xu, Chong Li, Hua Dong, Xinwei Wang. Thermal and electrical conduction in 6.4 nm thin gold films, Nanoscale, (05 2013): 4652. doi: 10.1039/c3nr00729d
08/28/2013	4.00	Nathan Velson, Xinwei Wang. Characterization of thermal transport across single-point contact between micro-wires, Applied Physics A, (09 2012): 403. doi: 10.1007/s00339-012-7177-y
08/28/2013	3.00	Shen Xu, Xinwei Wang, Ning Mei, Huan Lin. Thermal and Electrical Conduction in Ultrathin Metallic Films: 7 nm down to Sub-Nanometer Thickness, Small, (08 2013): 1. doi: 10.1002/smll.201202877
08/28/2013	2.00	Xuhui Feng, Guoqing Liu, Shen Xu, Huan Lin, Xinwei Wang. 3-dimensional anisotropic thermal transport in microscalepoly(3-hexylthiophene) thin films, Polymer, (02 2013): 1887. doi:
08/31/2014	5.00	Guoqing Liu, Shen Xu, Ting-Ting Cao, Huan Lin, Xiaoduan Tang, Yu-Qing Zhang, Xinwei Wang, Kenneth J. Breslauer. Thermally induced increase in energy transport capacity of silkworm silks, Biopolymers, (10 2014): 0. doi: 10.1002/bip.22496
08/31/2014	11.00	Shen Xu, Zaoli Xu, James Starrett, Cheryl Hayashi, Xinwei Wang. Cross-plane thermal transport in micrometer-thick spider silk films, Polymer, (04 2014): 0. doi: 10.1016/j.polymer.2014.02.020
08/31/2014	8.00	Shen Xu, Zaoli Xu, Xiaoduan Tang, Xinwei Wang. Energy transport in crystalline DNA composites, AIP Advances, (01 2014): 0. doi: 10.1063/1.4863924
08/31/2014	10.00	Huan Lin, Shen Xu, Yu-Qing Zhang, Xinwei Wang. Electron Transport and Bulk-like Behavior of Wiedemann–Franz Law for Sub-7 nm-Thin Iridium Films on Silkworm Silk, ACS Applied Materials & Interfaces, (07 2014): 0. doi: 10.1021/am501876d
12/08/2015	20.00	Shen Xu, Xinwei Wang. Across-plane thermal characterization of films based on amplitude-frequency profile in photothermal technique, AIP Advances, (10 2014): 0. doi: 10.1063/1.4898330
12/08/2015	18.00	Zhe Cheng, Zaoli Xu, Lei Zhang, Xinwei Wang, Xiao-Dong Wang. Thermophysical Properties of Lignocellulose: A Cell-Scale Study Down to 41K, PLoS ONE, (12 2014): 0. doi: 10.1371/journal.pone.0114821
12/08/2015	19.00	Zaoli Xu, Xinwei Wang, Huaqing Xie. Promoted electron transport and sustained phonon transport by DNA down to 10 K, Polymer, (11 2014): 0. doi: 10.1016/j.polymer.2014.10.016
12/08/2015	16.00	Jing Liu, Xinwei Wang. Characterization of thermal transport in one-dimensional microstructures using Johnson noise electro-thermal technique, Applied Physics A, (2 2015): 0. doi: 10.1007/s00339-015-9056-9

12/08/2015 17.00 Zhe Cheng, Zaoli Xu, Shen Xu, Xinwei Wang. Temperature dependent behavior of thermal conductivity of sub-5?nm Ir film: Defect-electron scattering quantified by residual thermal resistivity,
Journal of Applied Physics, (01 2015): 0. doi: 10.1063/1.4905607

12/08/2015 14.00 Yangsu Xie, Zaoli Xu, Shen Xu, Zhe Cheng, Nastaran Hashemi, Cheng Deng, Xinwei Wang. The defect level and ideal thermal conductivity of graphene uncovered by residual thermal reffusivity at the 0 K limit,
Nanoscale, (2015): 0. doi: 10.1039/C5NR02012C

12/08/2015 15.00 Zhe Cheng, Longju Liu, Shen Xu, Meng Lu, Xinwei Wang. Temperature Dependence of Electrical and Thermal Conduction in Single Silver Nanowire,
Scientific Reports, (6 2015): 0. doi: 10.1038/srep10718

12/08/2015 12.00 Zaoli Xu, Zhe Cheng, Jing Liu, Shen Xu, Xinwei Wang. Thermal Conductivity of Ultrahigh Molecular Weight Polyethylene Crystal: Defect Effect Uncovered by 0 K Limit Phonon Diffusion,
ACS Applied Materials & Interfaces, (12 2015): 0. doi: 10.1021/acsami.5b08578

12/08/2015 13.00 Yangsu Xie, Shen Xu, Zaoli Xu, Hongchao Wu, Cheng Deng, Xinwei Wang. Interface-mediated extremely low thermal conductivity of graphene aerogel,
Carbon, (11 2015): 0. doi: 10.1016/j.carbon.2015.11.033

TOTAL: **17**

Number of Papers published in peer-reviewed journals:

(b) Papers published in non-peer-reviewed journals (N/A for none)

Received Paper

TOTAL:

Number of Papers published in non peer-reviewed journals:

(c) Presentations

Number of Presentations: 0.00

Non Peer-Reviewed Conference Proceeding publications (other than abstracts):

Received Paper

TOTAL:

Number of Non Peer-Reviewed Conference Proceeding publications (other than abstracts):

Peer-Reviewed Conference Proceeding publications (other than abstracts):

Received Paper

TOTAL:

Number of Peer-Reviewed Conference Proceeding publications (other than abstracts):

(d) Manuscripts

Received Paper

TOTAL:

Number of Manuscripts:

Books

Received Book

TOTAL:

Received	Book Chapter

TOTAL:

Patents Submitted

Patents Awarded

Awards

Graduate Students

NAME	PERCENT_SUPPORTED	Discipline
Shen Xu	0.50	
Zaoli Xu	0.50	
Jing Liu	0.50	
Bowen Zhu	0.30	
Sandra Correa	0.50	
FTE Equivalent:	**2.30**	
Total Number:	**5**	

Names of Post Doctorates

NAME	PERCENT_SUPPORTED
FTE Equivalent:	
Total Number:	

Names of Faculty Supported

NAME	PERCENT_SUPPORTED	National Academy Member
Xinwei Wang	0.08	
Cheryl Hayashi	0.00	
FTE Equivalent:	**0.08**	
Total Number:	**2**	

Names of Under Graduate students supported

NAME	PERCENT_SUPPORTED
FTE Equivalent:	
Total Number:	

Student Metrics

This section only applies to graduating undergraduates supported by this agreement in this reporting period

The number of undergraduates funded by this agreement who graduated during this period:	0.00
The number of undergraduates funded by this agreement who graduated during this period with a degree in science, mathematics, engineering, or technology fields:.....	0.00
The number of undergraduates funded by your agreement who graduated during this period and will continue to pursue a graduate or Ph.D. degree in science, mathematics, engineering, or technology fields:.....	0.00
Number of graduating undergraduates who achieved a 3.5 GPA to 4.0 (4.0 max scale):.....	0.00
Number of graduating undergraduates funded by a DoD funded Center of Excellence grant for Education, Research and Engineering:.....	0.00
The number of undergraduates funded by your agreement who graduated during this period and intend to work for the Department of Defense	0.00
The number of undergraduates funded by your agreement who graduated during this period and will receive scholarships or fellowships for further studies in science, mathematics, engineering or technology fields:	0.00

Names of Personnel receiving masters degrees

NAME
Total Number:

Names of personnel receiving PHDs

NAME	
Zaoli Xu	
Shen Xu	
Total Number:	**2**

Names of other research staff

NAME	PERCENT_SUPPORTED
FTE Equivalent:	
Total Number:	

Sub Contractors (DD882)

1 a. University of California - Riverside

1 b. 200 University Office Building

Riverside CA 925210001

Sub Contractor Numbers (c): 421-20-52A
Patent Clause Number (d-1):
Patent Date (d-2):
Work Description (e): Spider silk collection, analysis, and further preparation for thermal characterization
Sub Contract Award Date (f-1): 7/1/14 12:00AM
Sub Contract Est Completion Date(f-2): 6/30/15 12:00AM

1 a. University of California - Riverside

1 b. 200 University Office Building

Riverside CA 925210001

Sub Contractor Numbers (c): 421-20-52A
Patent Clause Number (d-1):
Patent Date (d-2):
Work Description (e): Spider silk collection, analysis, and further preparation for thermal characterization
Sub Contract Award Date (f-1): 7/1/14 12:00AM
Sub Contract Est Completion Date(f-2): 6/30/15 12:00AM

Inventions (DD882)

Scientific Progress

See Attachment

Technology Transfer

ARO Final Project Report

Ultra-high Thermal Conductivity of Spider Silk: Protein Function Study with Controlled Structure Change and Comparison

Xinwei Wang/PI, Iowa State University
Cheryl Hayashi/co-PI, University of California-Riverside

1. Statement of the Problems Studied

In this project, we intend to address problems including: what are the mechanisms that enable protein structures to sustain fast phonon transport, what are the physics behind the structural change under stretching that makes the thermal conductivity to increase, and what are the protein structures in spider silk that favor the highest thermal transport. To answer these fundamental questions and lay the foundation for developing applications using the unique thermal transport properties of spider silks, the objectives of this proposal are develop a novel technology to characterize the thermal conductivity in the radial (cross-plane) direction of spider silks, unravel the mechanisms of ultra-high thermal conductivity sustained by the unique protein structure in spider silk, and discover the physics of thermal conductivity increase/tunability under controlled structure change.

2. Overall Scientific Accomplishments

In the past three years, we have conducted extensive research to study the structure of spider silks and investigate how the structure affects the silk's thermal transport. The comparison of thermal conductivity (κ) and structural information between the naturally spun and manually spun spider silks demonstrates that the alignment of the antiparallel β-sheet crystals in spider silks plays one of the most important roles in improving thermal transport. Various structural manipulations have been introduced by casting the silk protein into different shapes, varying the speed of manual silk spinning, using different silks from the same spider and silks from different types of spiders. The thin width of silks has been proved to significantly improve κ. The silks from the spiders in unhealthy conditions also showed a higher κ. Rough structures would enhance phonon scattering and thus lower κ. A small range of the variation of the spinning rate in producing spider silks would not obviously increase κ, when no significant shape change is induced. The organic solvent in silver paste involved in our experiment has little effect in decreasing κ. On the other hand, to go deeper into the nanoscale nature of the structure of spider silks, X-ray diffraction (XRD) has been employed to study the crystallite size of spider silks. Also a lab-developed thermal reffusivity theory has been employed to study thermal properties of spider silks at low temperatures down to 10 K. The crystallite size obtained through XRD and mean free path of the defect-induced phonon scattering are nicely consistent with each other.

3. Detailed Achievements

(1). Raman spectrum of spider silk (naturally spun)

Previous polarized Raman study of *Nephila clavipes* (*Nc*) silks showed that the 1230 cm^{-1} peak (Amide III in β-sheet crystal) and 1390 cm^{-1} (poly-Ala in β-sheet crystal) peak are tightly related to the β-sheet crystals along the axial direction of the silk fiber [1,2]. It can interpret the observed sound thermal conductivity in Huang's work. In that work, the Raman spectrum of the naturally collected *Nc* fiber showed two very strong peaks at both 1230 cm^{-1} and 1390 cm^{-1} (similar

intensity) though the excitation laser was circularly polarized (Fig. 1). These two peaks substantiated the highly ordered alignment of β-sheet crystals in Huang's sample. For comparison, the spectrum of the manually spun silk with a low thermal conductivity is also plotted in Fig. 1. It too exhibited two strong peaks at 1230 cm^{-1} and 1390 cm^{-1}. But the intensity of 1390 cm^{-1} peak was only one half of the intensity of 1230 cm^{-1} peak. This suggests that though the manually spun silk has a large amount of β-sheet crystals, the alignment along the axial direction is not as good as the natural silk and thus lowered the thermal conductivity.

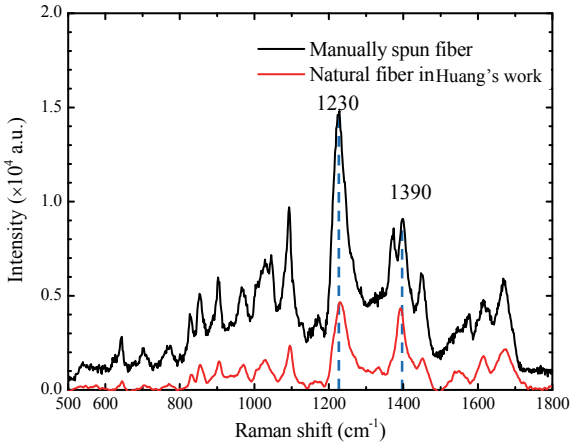

Figure 1. Raman spectra for naturally collected silk and manually spun silk of *Nephila clavipes*. Intensity is not available for direct comparison between the two spectra due to the different integration time in Raman experiment.

(2). Structure and thermal transport comparison study of spider silk fibers and films

This portion of the research focused on the relationship between thermal transport capacity and structure variation in spider silk films cast from natural spider silk protein (fresh films), processed spider silk protein (HFIP films), and in manually pulled spider silk fibers (fibers). Adult female *Nephila clavipes* and adult female *Latrodectus hesperus* (*Lh*) were studied. From their Raman spectra (Fig. 2) of all films and fibers, the *Nc* fiber was found to have only antiparallel β-sheets and random coils. The fresh films had more crystalline secondary protein structures such as β-sheets than the HFIP films. For *Latrodectus hesperus*, the films comprised α-helices and random coils, while the fiber had β-sheet crystals.

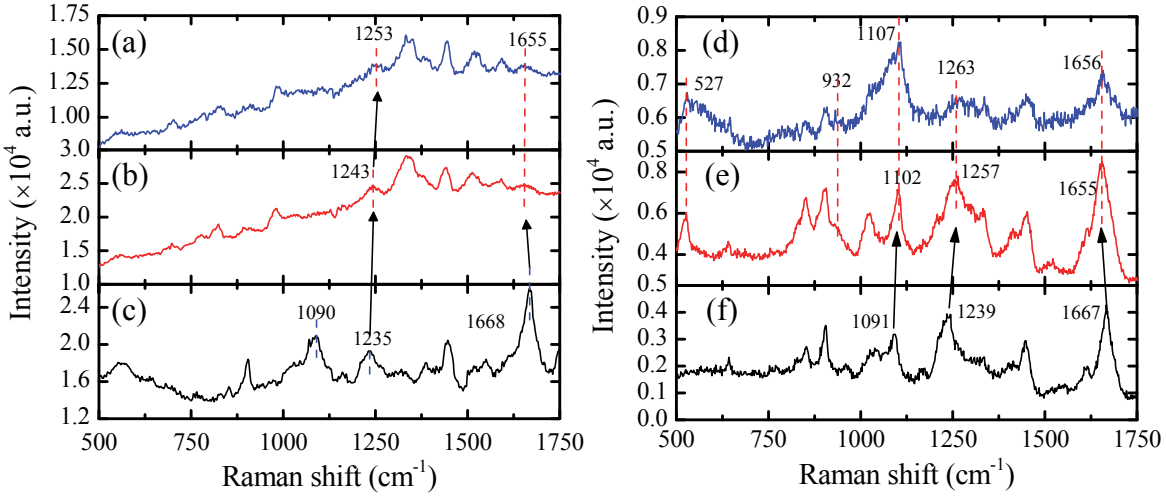

Figure 2. Raman spectra of *Nephila clavipes* samples: (a) HFIP film (blue line), (b) fresh film (red line) and (c) silk fiber (black line). Raman spectra of *Latrodectus hesperus*: (d) HFIP film (blue line), (e) fresh film (red line) and (f) silk fiber (black line).

The thermal properties were measured by using the photothermal (PT) and transient electro-thermal (TET) techniques and summarized in Tables 1 and 2. In *Nc* samples, both films and fibers had similar thermal conductivities around 0.34~0.40 W/m·K, though the fibers had more antiparallel β-sheets which are better in conducting heat than any other protein structures. This means these antiparallel β-sheets were randomly oriented in the fibers and had no contribution to improve thermal transport. The thermal conductivity of the *Lh* fiber (0.9~2.55 W/m·K) was significantly higher than that of *Lh* film samples (0.27~0.44 W/m·K). The highly oriented antiparallel β-sheets and few defects enhanced the thermal conductivity of the fiber. Also we found that for the fiber, when the diameter is thinner, the thermal conductivity will be improved significantly. The conclusion also applied to the comparison between the same types of silks or silks of different spider species. The thermal conductivity of the 0.5 μm *Lh* fiber was 2.55 W/m·K, about 183% higher than that of thicker fibers. We speculated that during the manual drawing process, the thinner fiber will experience significantly stronger surface tension effect, which helps significantly to improve the molecular alignment inside.

Table 1. Thermophysical properties determination based on phase shift and amplitude (PT).

		Phase shift fitting		Amplitude fitting	
Sample index	d (μm)	$\rho \cdot c_p$ (10^6 J/K·m^3)	k (W/m·K)	$\rho \cdot c_p$ (10^6 J/K·m^3)	k (W/m·K)
Nephila clavipes					
fresh1	18.58	1.57	0.365	1.53	0.547
fresh2	28.19	1.34	0.388	1.48	0.448
HFIP1	5.69	1.73	0.343	1.39	0.359
HFIP2-thick	17.34	1.57	0.404	1.38	0.610
Latrodectus hesperus					
fresh1	21.32	1.74	0.306	2.08	0.396
fresh2	6.53	1.78	0.355	1.68	0.397
HFIP1	3.39	1.14	0.435	1.20	0.668
HFIP2	2.24	1.37	0.270	1.55	0.264
HFIP3	2.06	1.31	0.280	1.67	0.270

Table 2. TET experimental data and calculated results for fiber samples.

samples	L (mm)	D (μm)	L^2/D (m)	$\alpha_{real+rad+gold}$ (10^{-6}m^2/s)	$\alpha_{real+rad}$ (10^{-6}m^2/s)	α (10^{-6}m^2/s)	k (W/m·K)
Nephila clavipes							
3m_sec.1	1.00	4.66	0.214	1.05	0.472		
3m_sec.2	1.42	4.61	0.436	1.21	0.642	0.276	0.370
3m_sec.3	1.66	4.61	0.596	1.41	0.810		
Latrodectus hesperus							
7D_sec.1	0.774	0.554	1.08	4.49	2.91	1.48	2.55
7D_sec.3	1.27	0.505	3.18	8.05	5.67		
2c_sec.1	0.915	1.55	0.539	1.82	1.05	0.530	0.900
2c_sec.3	1.85	1.58	2.17	3.5	2.63		
5k_sec.1	0.656	2.40	0.178	1.59	0.790		
5k_sec.2	1.07	2.22	0.519	1.8	0.990	0.570	0.980
5k_sec.3	1.64	2.27	1.19	2.49	1.72		

(3). Structure and thermal transport in silks spun by spiders of different health status

The effect of the health status of spiders when the silks were produced has been taken into consideration in this part. The tested samples were bridge fibers from a stressed *Nephila clavipes* individual, and a scaffold fiber from a sick *Nephila clavipes* individual. The words 'stressed' and 'sick' described the health conditions of the spider individuals kept in the laboratory. 'Stressed' denoted the spider not given food, water, or both, for 9 days prior to silk sample collection. 'Sick' meant the spider died in the cage, and afterwards the remaining silks were collected. Bridge and scaffold fibers are both similar to orb-web frame fibers, and are likely composed of silk protein from major ampullates (MA), but have different usages from the frame fibers. The bridge fibers consist of two major strands and the diameter of single strand ranged from 3.5 to 4.2 μm. The scaffold fiber consisted of four strands with an average diameter of 4.93 μm for a single strand. Table 3 gives the detailed sample parameters and experimental results.

Table 3. Sample parameters and Experimental results

Fibers	L (mm)	D (μm)	α (10^{-7}m^2/s)
Neph5stressed_bridge_c	0.746	4.21	4.26
Neph5stressed_bridge_f	4.809	4.24	10.2
Neph5stressed_bridge_g	4.903	3.54	15.8
Neph5stressed_bridge_i	5.476	3.87	9.87
Neph9sick_scaffold_a	0.549	4.93	6.13

An average thermal diffusivity of 1.2×10^{-6} m^2/s was determined for bridge fibers except 'Neph5stressed_bridge_c' which was speculated to be contaminated by the solvent of silver paste. The thermal diffusivity of the scaffold fiber from the sick spider is 6.1×10^{-7} m^2/s. All results were much higher than the previous test results for *Nc* MA fibers, whose thermal diffusivities were around 2.8×10^{-7} m^2/s. Up to this point, a conclusion could be drawn that when a spider's health condition is severely reduced, the silk it spins tends to have a much higher thermal diffusivity (thermal transport capacity).

Raman characterization was also carried out for all types (scaffold, gravity, bridge, and fuzz) and conditions (healthy, stress, and sick) of silks. All these silks exhibited similar Raman spectra as shown in Fig. 3 except the scaffold-sick silk fiber. The intensity of all peaks in the spectrum of scaffold-sick silk fiber was much higher than other silks although a shorter integration time (2 minutes) was used for this spectrum than others (5 minutes) in Fig. 3. This leads to a very strong conclusion that silks spun by sick spiders have more β-sheet crystals inside, and this structure is also better aligned along the axial direction. This helps explain the observation that the silks spun by sick spiders had a higher thermal diffusivity than that of healthy spiders.

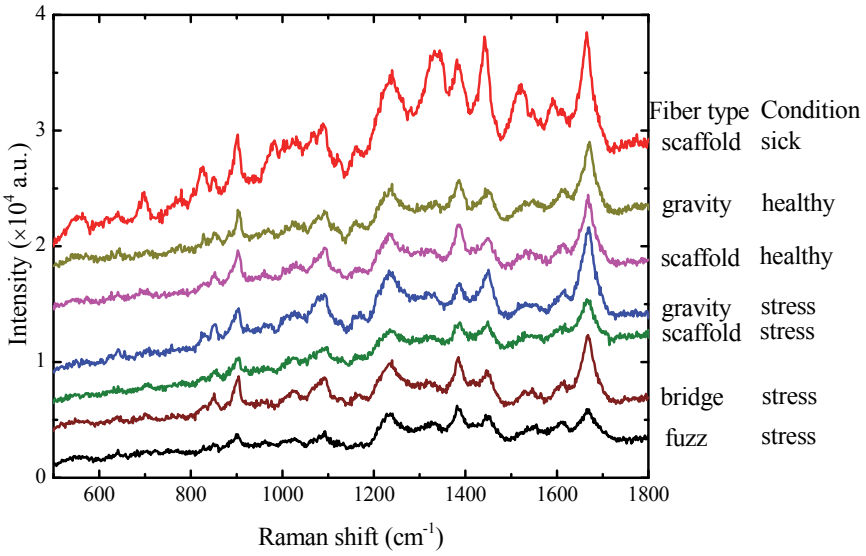

Figure 3. The spectra for *Nc* spider silks of different types and conditions.

(4). Effect of solvent-processing on the thermal conductivity of spider silk

To answer the raised speculation above whether the solvent in silver paste would change the internal structure of spider silks, we soaked the spider silks in two solvents and studied the thermophysical properties after solvent processed. First, we measured and compared α of spider silks soaked in ethanol with those of the non-processed samples using the TET technique. No obvious difference was observed in the appearance of the processed spider silks. α and κ for both the ethanol processed sample and the original sample are summarized in Table 4. Meanwhile, cryogenic TET measurements of these two types of silks were carried out from 290 K to 10 K. No significant difference existed in thermal reffusivity between the ethanol processed sample and the original sample. However, considering the statistical uncertainty, we can conclude that ethanol-processing indeed reduces the thermal reffusivity, which means the thermal conductivity is increased. Effect of acetone on k of *Nc* MA spider silks was also studied in the same procedures. α and κ of acetone processed spider silks and original samples are shown in Table 4. The result told no difference in κ between processed samples and original samples. Based on these results, we could conclude that the original structure in spider silk is already highly disorder. Though ethanol/acetone can break some H-bonds inside the silk protein, the overall thermal conductivity would not observably decrease.

Table 4. Thermal properties of ethanol processed spider silks compared with original samples

Thermal properties	Original samples			Ethanol processed samples*			Acetone-processed samples**		
	Nc-4x	*Nc*-44	*Nc*-41	*Nc*-4a	*Nc*-40	*Nc*-41	*Nc*-25	*Nc*-26	*Nc*-28
Thermal diffusivity ($\times 10^{-7}$ m^2/s)	4.80	6.71	5.44	6.00	5.18	5.34	5.62	4.78	5.06
Thermal conductivity (W/m·K)	0.86	1.20	0.95	1.20	1.04	1.12	1.06	0.91	0.96

**Nc*-4a, *Nc*-40 and *Nc*-41 are immersed in ethanol for over 12 hours, followed by a 1-hour air drying.
***N*c-25, *N*c-26 and *N*c-28 are processed with a 2-hour total immersion in acetone and 1 hour air drying

(5). Thermal transport in *Loxosceles laeta* silk and effect of spinning speed on α

The thermal diffusivity of another type of spider (*Loxosceles laeta*, *Ll*) silk was studied in this section. This was the first time study of the thermal transport in this very special type of spider silk. *Ll* MA silks have a ribbon-like shape with a very thin thickness, which is very different from that of orb-weaver spiders: *Nephila clavipes* and *Latrodectus hesperus*. An *Ll* silk with an average width of 5.80 μm, a length of 0.831 mm and a thickness of 84.6 nm was used for the TET characterization. The real thermal diffusivity of this *Ll* silk was 1.97×10^{-6} m^2/s. This value was much higher than the α of *Nc* silks (MA fiber, around 2.6×10^{-7} m^2/s). The extrusion and solidification of the *Ll* silk fiber during spinning play important roles in determining the internal structures of the silk fiber, for it has a large surface/volume ratio. Strong surface tension force and shear stress during spinning could help a great deal to align protein crystals in the silk, thereby leading to significantly improved thermal transport capacity.

We then measured the thermal diffusivity of the spider silks spun at high and low rates, respectively, and tried to find whether the spinning rate affected the thermal diffusivity of spider silks. *Nc* MA silks spun at the rates of 4.28 cm/s (slow) and 30.81 cm/s (fast), and *Ll* MA silks spun at 9.78 cm/s (slow) and 24.67 cm/s (fast) were measured. Raman spectra of *Nc* MA silks are shown in Fig. 4(a). Figure 4(b) shows Raman spectra of *Ll* MA silks. No significant difference was found in these spectra and their internal crystalline structures.

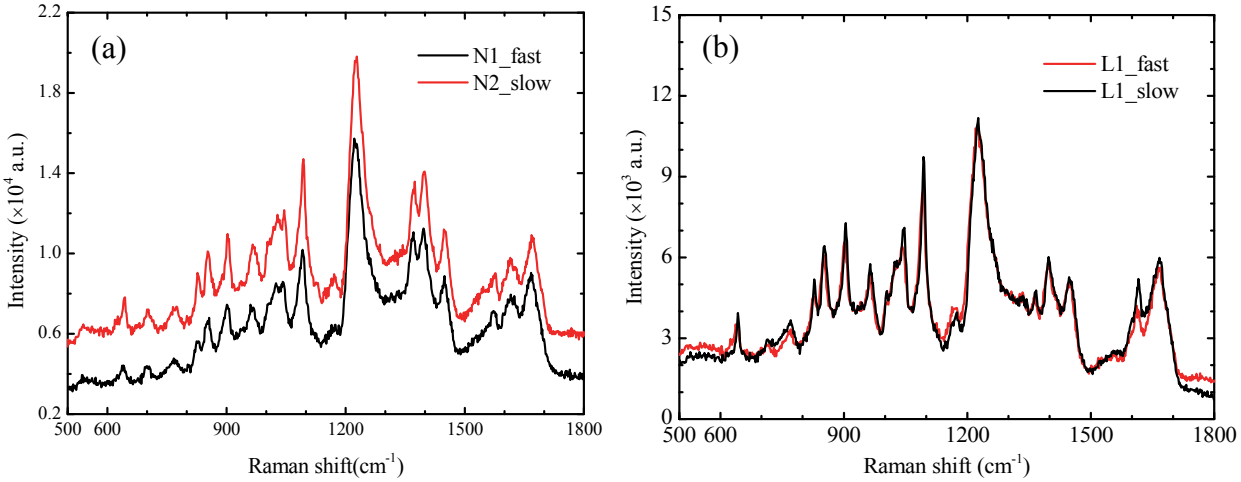

Figure 4. Raman spectra of *Nephila clavipes* (a) and *Loxosceles laeta* (b) major ampullate silks spun at different rates.

Their thermal diffusivity ranged from 3.44 to 4.83×10^{-7} m^2/s for *Nc* samples and 3.51 to 4.48×10^{-7} m^2/s for *Ll* samples in the TET measurement. We concluded that the spinning rate of silk collecting has (negligible) little effect on the thermal diffusivity for both *Nc* and *Ll* spider silks. This conclusion conditionally applied to the spinning rate we studied here: 4.28~30.81 cm/s. In this spinning rate range, the diameter of silks showed very little variation from sample to sample. This confirmed that the spinning rate did not change the morphology so much. So it is physically reasonable that the thermal diffusivity varies little among the samples. Our speculation is that the structure, morphology, and thermal diffusivity of spider silks would show obvious change when the spinning rate is varied more, e.g. much faster than 30.81 cm/s.

(6). Protein β-sheet crystal size: first time quantitative experimental evidence

A scaffold fiber from a sick *Nephila clavipes* individual was measured in a cryogenic system from room temperature down to ~50 K using the TET technique. The temperature was precisely monitored by a temperature controller. Figure 5(a) shows the variation of thermal diffusivity with temperature for the scaffold fiber: The thermal diffusivity increases with decreasing temperature. This was due to the decrease of phonon-phonon scatterings. As temperature dropped, short wavelength phonons were frozen and only long wave phonons were excited. The reduced number of phonons resulted in less scatterings. This contributed to the increase of phonon mean free path, relaxation time and subsequently thermal diffusivity.

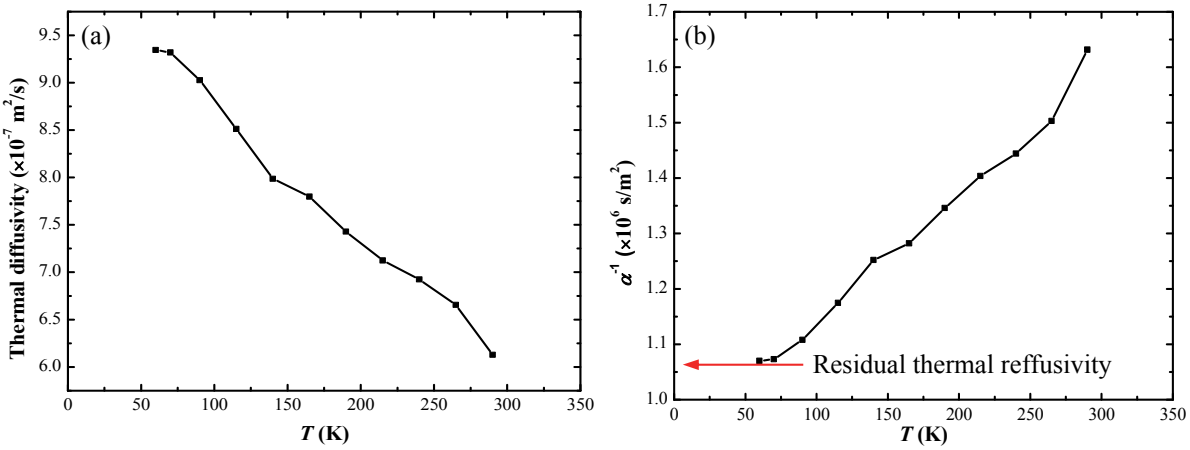

Figure 5. Variation of thermal diffusivity (a) and the thermal reffusivity (b) with temperature for the scaffold fiber from a sick *Nephila clavipes* individual.

Using the single relaxation time approximation, we introduced the inverse of phonon thermal diffusivity as a new parameter: thermal reffusivity (Θ). This parameter was used to identify the thermal resistivity in the fiber that was raised by fiber structure imperfections and by phonon-phonon scatterings. Figure 5(b) shows the variation of thermal reffusivity with temperature for the scaffold fiber. It is clearly seen that α^{-1} increases almost linearly with increasing temperature within the temperature range we use. This is due to the fact that phonon density increases almost linearly with temperature when the temperature is not very low. The residual part α_0^{-1} is about 1.05×10^6 s/m^2. Using an average phonon velocity of 630 m/s for spider silks, we had the relaxation time $\tau_0 = 7.2\times10^{-12}$ s and the characteristic size of the mean free path of phonons was 4.5 nm. It was intrinsically the β-sheet crystal size in the silk.

(7). Crystalline structure of spider silk uncovered by X-ray diffraction

The crystalline structures of three bundles of spider silks were characterized by XRD. The XRD spectra are shown in Fig. 6. A weak peak is observed when 2θ (θ: the incident angle) is 20.3° in Fig. 6(a). The corresponding crystallite size is calculated to be 36 Å. The XRD spectrum for sample *Lh*-1 in Fig. 6(c) demonstrates no peak. From Figs. 6(a), (b) and (c), it can be concluded that the crystalline regions (or at least visible ones) only exist in some spider silks. The crystallite size of *Nc*-1 is consistent with the mean free path of defect-phonon scattering of *Nc*-4. In Fig. 6(b), although the spectrum is also for the *Nc* MA silk, the peak is very weak, barely distinguishable around 20.3°. Note samples *Nc*-4 and *Nc*-1 are not from the same batch of

collection. So it is true that silks from different spiders, even the same species, could vary a lot in crystalline structure.

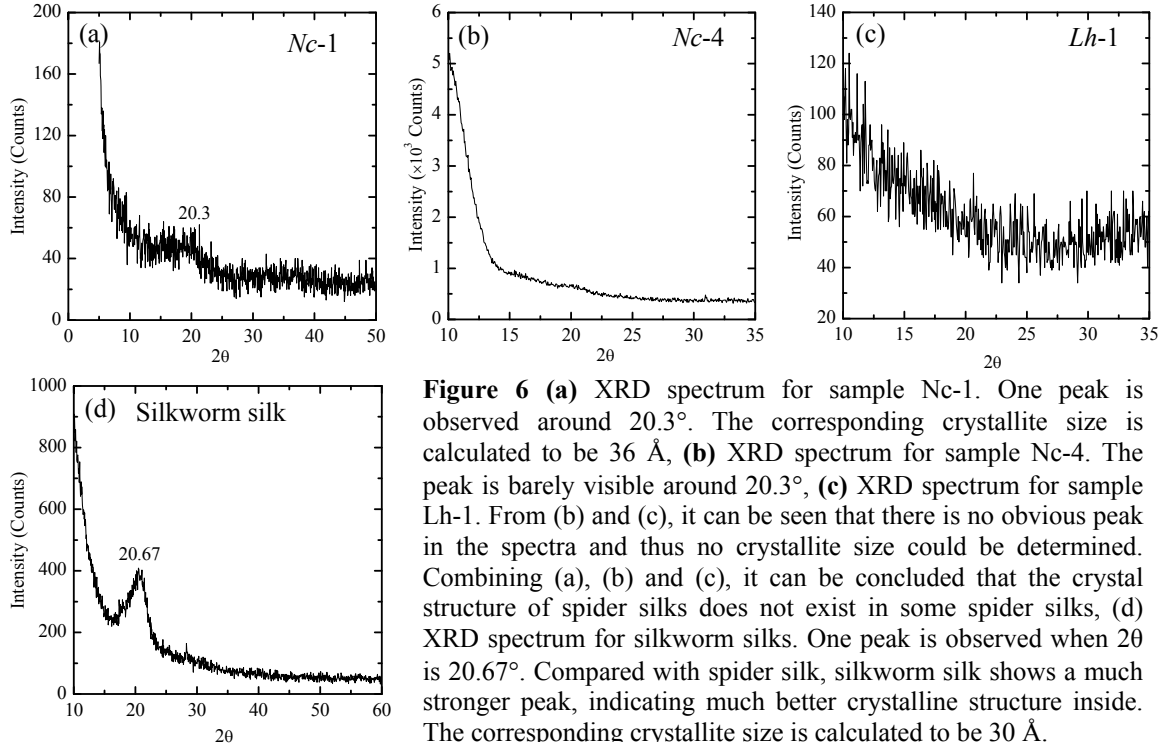

Figure 6 (a) XRD spectrum for sample Nc-1. One peak is observed around 20.3°. The corresponding crystallite size is calculated to be 36 Å, **(b)** XRD spectrum for sample Nc-4. The peak is barely visible around 20.3°, **(c)** XRD spectrum for sample Lh-1. From (b) and (c), it can be seen that there is no obvious peak in the spectra and thus no crystallite size could be determined. Combining (a), (b) and (c), it can be concluded that the crystal structure of spider silks does not exist in some spider silks, (d) XRD spectrum for silkworm silks. One peak is observed when 2θ is 20.67°. Compared with spider silk, silkworm silk shows a much stronger peak, indicating much better crystalline structure inside. The corresponding crystallite size is calculated to be 30 Å.

The α of the *Nc*-4 MA silks was measured using our TET technique from room temperature down to almost 10 K. The thermal reffusivity is determined to be 1.55×10^{6} s/m^2. The relationship between the residual thermal reffusivity, mean free path of defect-induced phonon scattering (l_0) and phonon velocity (v) could be depicted as $\Theta_0=3/(vl_0)$. When the average phonon velocity of spider silk was estimated as 630 m/s, the mean free path due to defect-phonon scattering was correspondingly calculated to be 3.07 nm. This value is consistent with the crystallite size (36 Å) obtained through XRD. In some spider silks, even though there were β-sheet crystals in it, XRD could not detect them when the β-sheet crystals had relatively bad alignment. However, the defect-phonon scattering mean free path could be evaluated through the method of thermal reffusivity, which can directly show the crystallite size of β-sheet crystals in spider silks.

(8). Thermal transport in male *Nephila clavipes* fibers: evidence of structural effect

We also measured the thermal diffusivity of the spider silks from male *Nephila clavipes* (M*Nc*) and tried to find out whether the structure had effect on the thermal diffusivity of spider silks. This was the first time study of thermal transport in M*Nc* fibers. Sample M*Nc*_2a and M*Nc*_3b were involved in the study. M*Nc*_2a was composited of a single filament. It had a length of 1.14 mm and a width of 1.07 μm and its measured α_{real} was 5.78×10^{-7} m^2/s. M*Nc*_3b, however, was a twist bundle of six filaments and had a rougher surface than M*Nc*_2a. It had a total width of 3.41 μm and a length of 1.18 mm. Its determined α_{real} ($=4.57\times10^{-7}$ m^2/s) was lower than M*Nc*_2a. The structure difference would affect the fiber's overall thermal diffusivity even for the fiber from the same spider, for the reason that a rough structure changes the phonon scattering a lot, giving low

thermal transport capacity.

(9). Thermal transport in silkworm silks: comparison study

A systematic work was conducted to study the thermal transport in silkworm silks and how the heat treatment could affect the thermal diffusivity/conductivity. This study was intended to provide an excellent comparison to understand how the protein structure determines the thermal transport capacity. Three types of fibroin degummed mild (type 1), moderate (type 2), to strong (type 3) were investigated. The thermal diffusivity in the axial direction increased against temperature used in heat treatment for the three types of samples [Fig. 7(a)]. After heat treatment (from about 140 °C to about 220 °C), the thermal diffusivity of silk fibroin type 1, 2 and 3, increased as high as 37.9%, 20.9% and 21.5%, respectively. No obvious difference in morphology was observed in the measured location on the fibers before and after heat treatment. The Raman spectrum comparison [Fig. 7(b)] indicates structural transformation from amorphous to crystalline. Due to the close packing of the more adjacent laterally ordered regions, the number and size of the crystalline regions of Bombyx mori silk fibroin increased by heat treatment. As a result, the thermal diffusivity of the samples was significantly improved.

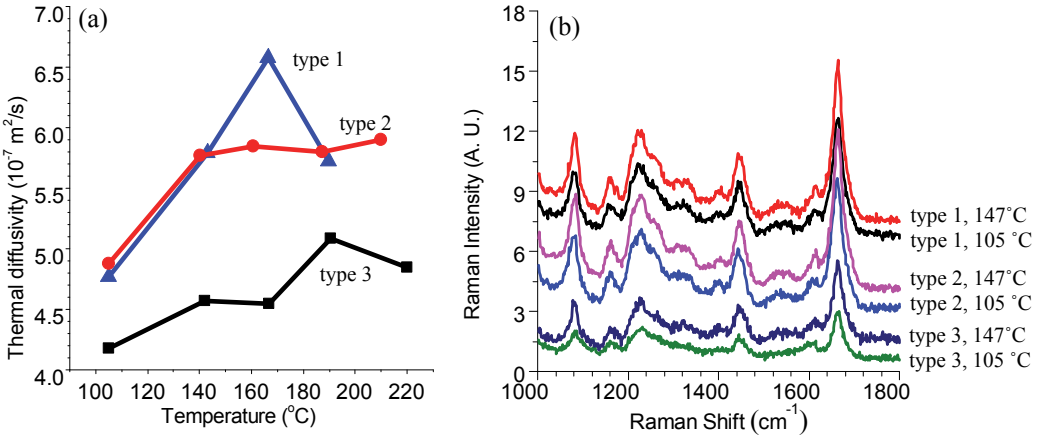

Figure 7. (a) Thermal diffusivity of silkworm silk after heat treatment at different temperatures, (b) Raman spectrum comparison of the silkworm silk treated at 105 and 147 ˚C.

(10). Crystallite size in silkworm silk and its Debye temperature

For comparison with spider silk, we also studied the crystallite size in silkworm silk using XRD and the thermal reffusivity (Θ) theory. Figure 8 shows the trend of Θ of silkworm silk varying with temperature from RT to 50 K: Θ decreases with decreasing temperature. Through fitting the curve with $\Theta = \Theta_0 + B \times e^{-\theta/2T}$, we had the Θ_0 determined as 1.63×10^6 s/m^2 and θ as 696.5 K. Θ_0 reflects the defect-induced phonon scattering level in the samples, and θ is the Debye temperature. When the average phonon velocity takes 630 m/s, the corresponding mean free path of defect-phonon scattering (l_0) was 2.92 nm. The XRD spectrum for silkworm silk [Fig. 6(d)] shows a clear peak at 2θ of 20.67º. The corresponding crystallite size was calculated to be 30 Å. It was consistent with the mean free path of defect-induced phonon scattering determined from the thermal reffusivity. It was also interesting to see the XRD peak location of silkworm silk (20.67º) is very close to that of spider silk (20.3°). This concluded that the β-sheet crystals in silkworm silk and spider silk share the similar lattice spacing.

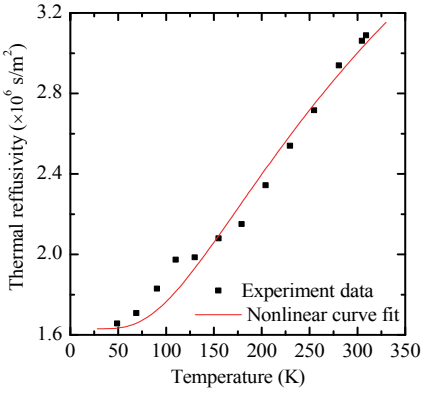

Figure 8. Thermal reffusivity of silkworm silk against temperature. The residual thermal reffusivity and Debye temperature are fitted to be 1.63×10^6 s/m^2 and 696.5 K. When the average phonon velocity is estimated as 630 m/s, the mean free path of defect-phonon scattering is determined to be 2.92 nm. This value is very close to the crystallite size uncovered by XRD.

(11). Reduced thermal/electrical conductivity in ultra-thin metallic films on spider silks

In the TET experiments to characterize the thermal diffusivity and conductivity of spider silks and such biomaterial or polymer fibers, a metallic film (tens of nm) was usually coated on the sample to facilitate the measurement. Precise knowledge about the thermal conductivity of this thin metallic film (Ir, used in our lab) was critical to evaluate the effect of the metallic coating on the final measurement results. The part of the work was critical to the overall project. The thermal and electrical conductivities (κ and σ) of Ir films with an average thickness from 7 nm down to 0.6 nm were found reduced by more than 59% and 82% compared to bulk Ir. The much stronger reduction in σ significantly increased the Lorenz number to around $6\sim8\times10^{-8}$ W·Ω·K^{-2} or larger, about twofold increase from the bulk value. This result has been using in all our later studies.

(12). New technique development for 3D anisotropic thermal transport characterization

This work was our first try to characterize the anisotropic thermal transport in polymers, such as silks. A new pulsed laser-assisted thermal relaxation (PLTR2) technique has been developed and was capable of studying both in-plane and out-of-plane thermal transport. Instead of using silks, we used P3HT films what are abundant for research. This material presented an anisotropic thermal conductivity with an anisotropy factor of about 2 to 4. This work provided the great foundation for future research to study the anisotropic thermal transport in silk fibers and silk films. Also in this work, we have assessed the feasibility of using polarized Raman to characterize the anisotropic structure (molecular alignment), and have achieved success.

References

1. Marie-Eve Rousseau, Thierry Lefèvre, Lilyane Beaulieu, Tetsuo Asakura, and Michel Pézolet. *Biomacromolecules*,(2004), 5, 2247-2257.

2. Marie-Eve Rousseau, Thierry Lefèvre and Michel Pézolet. *Biomacromolecules* (2009), 10, 2945–2953.